

Transfer Printing of Metal Nanoring and Nanodot Arrays for Use in Catalytic Reaction

S. H. Lee,^{ab†}, S. M. Choi,^{c†} S. Yoon,^a H. Jung,^a G. Y. Jung,^a B. K. Cho,^a and W. B. Kim^{*ab}

^aSchool of Materials Science and Engineering, Gwangju Institute of Science and Technology (GIST),
Gwangju 500-712, Republic of Korea.

^bResearch Institute for Solar and Sustainable Energies, Gwangju Institute of Science and Technology
(GIST), Gwangju 500-712, Republic of Korea.

^cSurface Technology Division, Korea Institute of Materials Science (KIMS), Changwon 641-010,
Republic of Korea.

* Address correspondence to wbkim@gist.ac.kr.

† These authors contributed equally.

Experimental section

Fabrication of vertically aligned CNT and CNP arrays. The two types of stamps were composed of vertical carbon-based nanostructure arrays prepared from porous alumina templates (see Figure S3 of the Supplementary Information). The fabrication of the nanostamps began with the production of AAO templates formed by a two-step anodization process. The electropolished Al plates were first anodized in a 0.3 M $\text{H}_2\text{C}_2\text{O}_4$ electrolyte under a constant potential of 40 V. After removal of the irregular alumina layers formed in the 1st anodization process, the 2nd anodization was carried out under the same conditions to produce AAO templates with hexagonally arranged porous channels at a high pore density of $1 \times 10^{10} \text{ cm}^{-2}$. A pore-widening process involving etching in H_3PO_4 , CrO_3 , and DI water (6:1.8:92.2 wt%) at 60 °C for 70 s was used to increase the original pore dimensions to ca. 65 nm in diameter. Carbon layers were deposited within the AAO channels by thermal chemical vapor deposition (CVD) at 600 °C without the use of metal catalysts. A mixed gas flow of C_2H_2 (20 sccm) and NH_3 (80 sccm) was introduced for 6 h as a feedstock for the formation of the carbon layers. To eliminate surface carbon layers deposited on the AAO during the CVD process, an Ar ion milling process was employed. The tip morphologies of the carbon nanostamps were modulated by adjusting the ion milling process. The ring-shaped tips were produced by milling for ca. 3 min, whereas the dot-shaped tips were formed by longer milling than 8 min. After the Ar ion milling step, the vertically aligned carbon nanostructures were created by chemical wet etching in phosphoric acid mixture solution to remove the alumina phase. The exposed height of the both stamp types was ca. 60 nm, which was precisely engineered by a 10 min etch.

Printing of metal ring and dot catalyst nanoarrays. Metal layers (Pt and Au) were first deposited on the CNT and CNP stamp tips. Then a thin Ti layer (ca. 1 nm) was loaded on the metal layers using an E-beam process. The metal-loaded stamps were placed directly on ITO substrates with application of the proper external pressure (0.5 ~ 1.0 MPa) for less than 5 s. This resulted in formation of metal nanoring and nanodot catalyst arrays over ITO substrates. The printing process was carried out under ambient conditions.

Evaluation of the electrocatalytic properties of the printed metal ring and dot catalysts. All electrochemical measurements were carried out by CV using a Solartron Analytical instrument (AMETEK model 1470E). The half-cell system was composed of an ITO glass working electrode that contained the printed metal nanoring and nanodot arrays, a platinum mesh counter electrode, and an Ag/AgCl reference electrode containing a saturated KCl solution. The mass of the printed Pt and Au catalysts was measured using a microbalance (Sartorius microbalance M3P). The CV characterization of the printed Pt nanorings and Pt nanodots was carried out in the potential range of -0.2 to 1.0 V at a scan rate of 100 mV/s in an ultra-high purity N_2 -purged 0.5 M H_2SO_4 electrolyte solution for hydrogen adsorption/desorption reaction and in a 2.0 M CH_3OH + 0.5 M H_2SO_4 electrolyte solution for methanol electrooxidation. CO stripping voltammetry experiments for the Pt nanorings and Pt nanodots were carried out in a 0.5 M H_2SO_4 electrolyte solution at room temperature. A gas-sealed glass cell with a gas inlet and outlet was used. The CO gas (99% purity) was introduced into the electrolyte solution at a constant CO flow rate of 20 sccm for 10 min. A controlled potential of 50 mV was applied to the working electrode for CO adsorption. A gas flow was converted into 100 sccm N_2 gas for 20 min to remove the CO molecules that might be dissolved in the solution or physically adsorbed on the electrode surfaces. CO stripping voltammetry was then performed over a potential range of -0.2 to 1.0 V at a scan rate of 100 mV/s. A comparison of the catalytic behaviors of the printed Au nanorings and the printed Au nanodots was performed using CO electrooxidation voltammetry in an ultra-high purity N_2 -purged 50 ml KOH electrolyte over a potential range of -0.4 to 0.6 V at a scan rate of 100 mV/s. After the KOH electrolyte was saturated with CO gas for 40 min, the CV test was carried out for a constant CO gas feed of 20 sccm through the inlet line.

The detailed structures of the CNTs and CNPs:

The illustrations of Figures S1a-b further describe the detailed structures of the CNTs and CNPs. The backbones of both the CNT and CNP arrays are composed of tubular walls with the hollow center, but they have the distinct tip morphologies. The transmission electron microscopy (TEM) images in insets of Figures S1a-b show the actual CNT and CNP structures, where the TEM samples were prepared by separating the CNTs and CNPs from the AAO templates via chemical etching. The distinguished contrast between the outer walls and the empty core spaces strongly shows that both the CNTs and CNPs consist of tubular nanostructures with wall thicknesses of ca. 10 nm, which is quite reasonable because the carbon deposition conditions on the AAO pore channels are exactly same for both types of stamps. The main difference between the stamps is their tip morphology (i.e., open vs. closed ends), which can be explicitly observed in the inset images of Figures S1a-b.

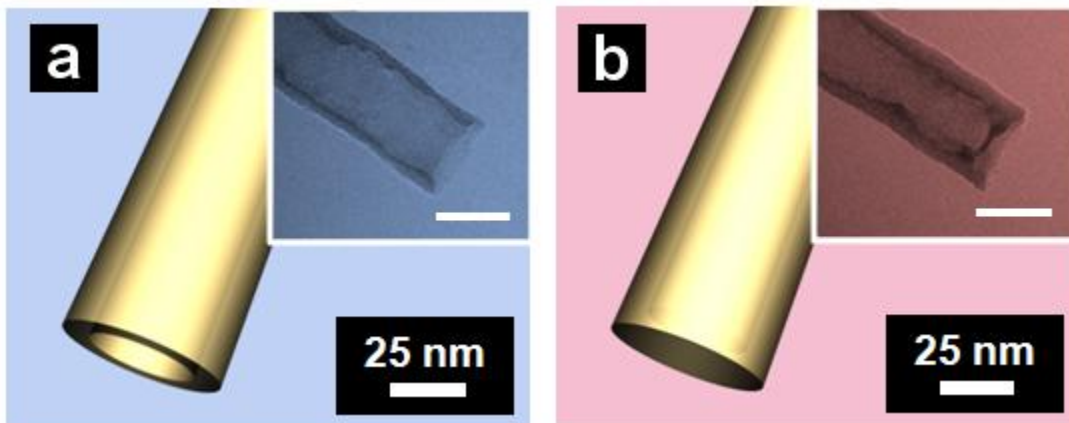


Fig. S1 Illustrations for the detailed inner structures of (a) the CNTs and (b) the CNPs. The TEM inset images represent the backbone structures and tip morphologies of the CNT and the CNP stamps. All scale bars in the insets are 50 nm.

The Raman, SAED, and HRTEM measurements for the stamps:

We investigated the detailed properties of the CNTs and CNPs using Raman spectroscopy, selective area electron diffraction (SAED), and high-resolution TEM (HRTEM), all of which provide information with respect to the material nature and crystallinity. The Raman spectrum in Figure S2a shows two strong peaks at approximately 1370 and 1590 cm^{-1} , which closely match with the D-band of amorphous carbon and the G-band of graphite, respectively. The peak intensity ratio of the G-band to the D-band is approximately 1.19, indicating that these nanostructures are composed of graphitic substances. The SAED pattern (Figure S2b) indicates that the carbon nanostructures consist of very small-sized grains or amorphous surfaces. The inset of Figure S2b shows a representative HRTEM image of individual magnified CNTs and CNPs, indicating that these nanostructures are composed of stacks of a number of flakes. Based on these data, it appears that the CNTs and CNPs consist of stacks of graphite flakes with very small crystal grains or amorphous surfaces.

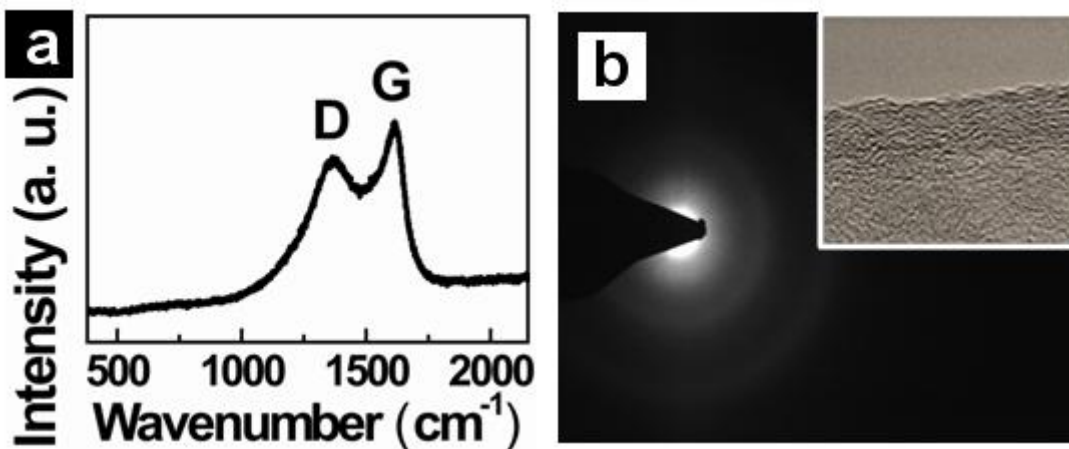


Fig. S2 Representative analytic results of the stamps used in this experiment: (a) Raman spectrum, (b) SAED patterns. The inset image shows HRTEM image for the carbon nanostructure walls.

Fabrication of the CNT and CNP stamps:

The illustrations in Figures S3a-c describe the fabrication procedures for the CNT and CNP arrays, with a particular emphasis on the difference in stamp preparation that generates the two different tip morphologies. The fabrication of the CNT and CNP stamps begins with the preparation of the AAO templates (left image of Figure S3a) that enable the stamp tips to be aligned with vertical orientation in hexagonal arrays, while sustaining the original morphology of the carbon arrays under applied contact pressure during printing. Carbon layers are then deposited over the AAOs by thermal CVD. The carbon deposition conditions for the CNTs and CNPs are completely identical (right image of Figure S3a). To release the aligned carbon nanostructures from the AAO template, the surface carbon layers must first be eliminated because these surface carbons protect the AAO layer from chemical etching. We employed an Ar ion milling process to remove the surface carbons from the AAO. Importantly, the tip morphologies of the nanostamps are precisely determined by the processing conditions during the ion milling. As seen in the schematic diagrams of Figure S3b, the tip morphologies are controlled simply by adjusting the milling time. If milling is carried out an appropriate time (e.g., approximately 3 min in this work), the surface carbon layers are removed (left side of Figure S3b), and thus CNT arrays with the ring-shaped open ends appear after selective etching of the AAO layers (left side of Figure S3c). However, if excessive milling (more than 8 min) is committed, the tips of the carbon nanostructures appear to be crushed and clogged (right side of Figure S3b), and therefore CNP arrays with the dot-shaped closed tips are produced (right side of Figure S3c). Except for the milling time, other milling conditions were constantly maintained. Figures S3d-f shows typical SEM images corresponding to the illustrations in Figures S3a-c. Figure S3d shows the original AAO templates (left side) and the carbon-deposited AAO templates from the thermal CVD process (right side). The carbon nanostructures perfectly replicate the original morphology of the AAO pore channels. The SEM images in Figures S3e-f show that the modification of the stamp tip morphologies is strongly dependent on the milling condition. With proper milling, the surface carbon is appropriately eliminated and open ends are

maintained (left side of Figure S3e). After selective etching of the AAO layers, the CNT stamps can be prepared (left side of Figure S3f). However, different milling processes lead to the collapse of the tips of the nanostructures (right side of Figure S3e). This allows the CNP stamps with closed tips to be produced (right side of Figure S3f). Controlling the stamp tip morphology via Ar ion milling provides two types of stamps for metal nanoring and nanodot printing.

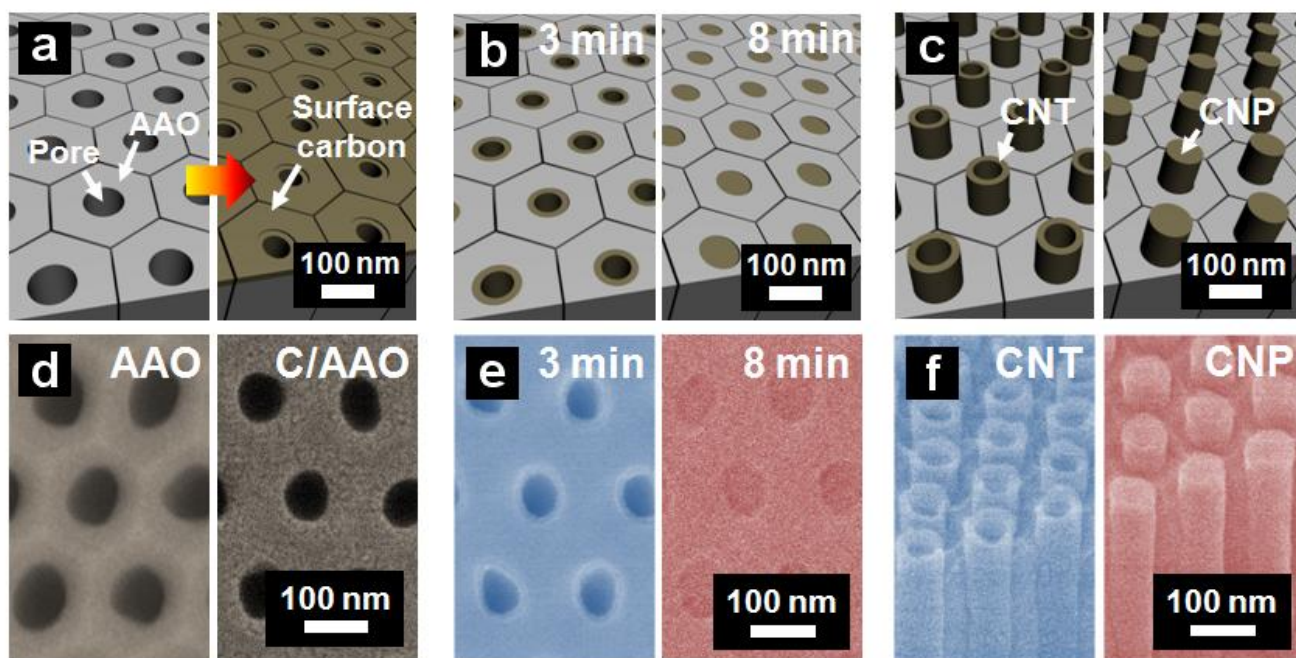


Fig. S3 Diagrams (a-c) depict the fabrication processes for the CNT and CNP stamps. (a) Preparation of AAO templates under controlled electrochemical conditions (left side) and deposition of hydrocarbon sources on the channel walls of the AAOs (right side). (b) Removal of carbon layers deposited on the AAO surfaces by Ar ion milling process. (c) Exposure of the vertically aligned CNT and CNP arrays by selective etching of the AAO surfaces. (d) SEM images show the configuration of the AAO template (left side) and the carbon layers deposited on the AAO by thermal CVD (right side). (e) Suitable milling processes (approximately for 3 min) allow carbon layers deposited on the AAO surface to be removed, thus the original tube tip of the carbon nanostructures within the AAO channels remains intact (left side). However, excessive milling (more than 8 min) causes the collapse of the tips (right side). (f) After selective etching of the AAOs, the CNT and CNP stamps are complete.

The deposition of metal layers on the tips of the CNT and CNP stamps:

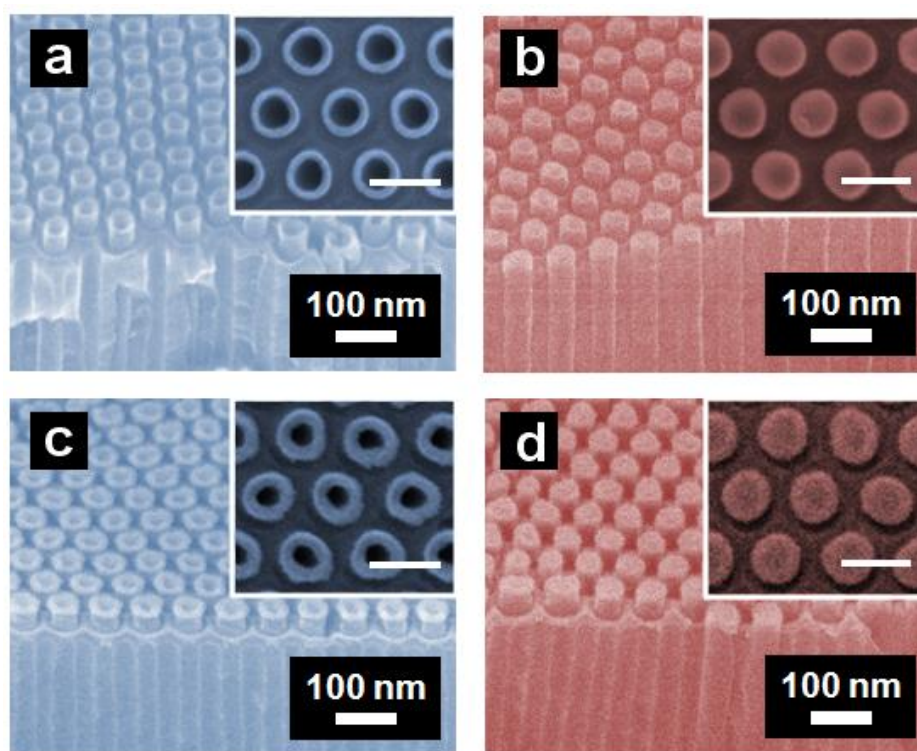


Fig. S4 SEM images for the preliminary morphologies of (a) the CNTs and (b) the CNPs. SEM images for the deposition of metal layers and adhesion-enhanced Ti layers on (c) the CNTs and (d) CNPs. The insets show the magnified images, and all scale bars in the insets are 100 nm.

The Pt nanoring and nanodot arrays printed over large substrate areas:

Figures S5a-b show the uniform distribution of numerous Pt nanoring and nanodot arrays over ITO substrates by the printing process. The brighter regions display the presence of the printed Pt arrays on substrates, whereas the darker regions indicate several defect sites, in which the metal arrays were not transferred. We speculate that the involvement of these defects might be attributed to the surface roughness of the ITO glasses, which can hinder the perfect contact between the stamp tips and substrates. Although some defects exist in this work, still a huge amount of metal ring and dot arrays with a narrow size distribution are well aligned over large substrate areas.

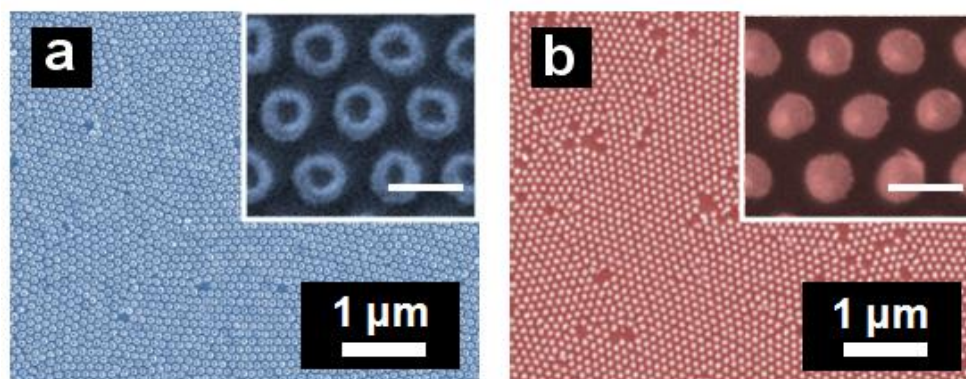


Fig. S5 SEM images of (a) the Pt nanorings and (b) the Pt nanodots printed over the ITO glasses. The insets show the magnified views of these printed nanoarrays. The scale bars in the insets are 100 nm.

The surface/volume ratio of the ring and dot arrays:

The model for the surface/volume ratio of the ring and dot structures can theoretically support the factor that the ring-shaped catalysts have much higher catalytic activity than the dot-shaped catalysts because of the larger active surface of the ring structure. In this model, the ring catalysts are considered as the torus shape, while the dot catalysts are regarded as the hemisphere shape as illustrated in Figure R1. The surface and volume of corresponding ring- and dot-shaped structures can be calculated by the following equations.

$$\text{The surface area of the torus: } \pi^2(r^2 - r_1^2)$$

$$\text{The volume of the torus: } \frac{1}{4}\pi^2(r^2 - r_1^2)(r - r_1)$$

$$\text{The surface/volume ratio of the torus: } \frac{4}{(r - r_1)}$$

$$\text{The surface area of the hemisphere: } \frac{1}{2}(4\pi r^2)$$

$$\text{The volume of the hemisphere: } \frac{1}{2}\left(\frac{4}{3}\pi r^3\right)$$

$$\text{The surface/volume ratio of the hemisphere: } \frac{3}{r}$$

Here, r indicates the outer radius of the ring and dot structures, and r_1 is the inner radius of the ring structures (refer to the graphical illustration of Figure S6). Based on the SEM images of the insets in Figure S6, the real values of the r and r_1 can be estimated, where r and r_1 are ca. 32.5 nm and ca. 16 nm, respectively. Therefore, the surface/volume ratio of the torus and the hemisphere is ca. 0.242 and ca. 0.092, respectively, indicating that the ring catalysts have much higher active surface than the dot catalysts.

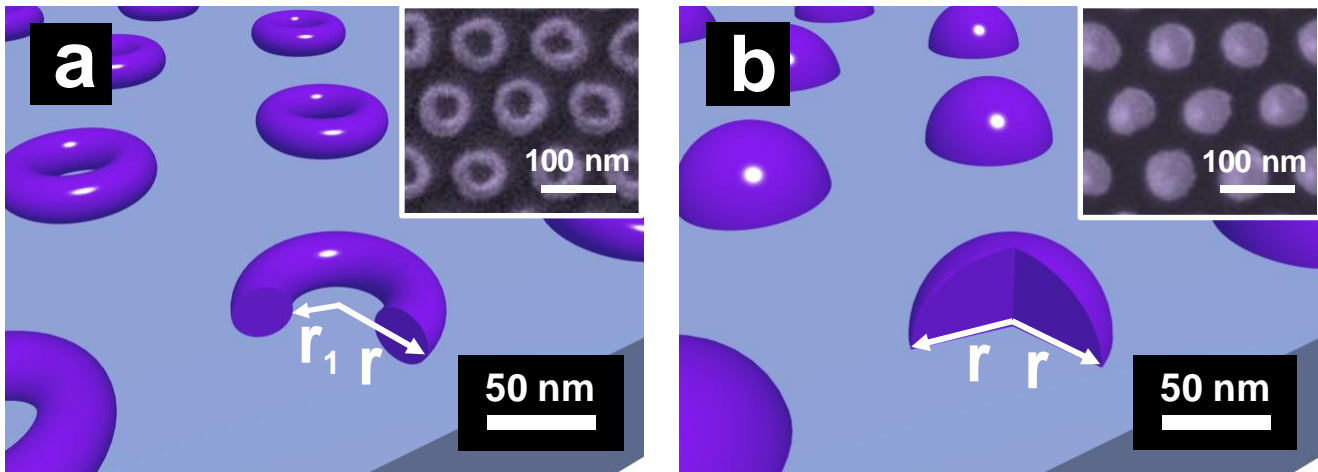


Fig. S6 Graphical illustration of the printed (a) nanoring and (b) nanodot arrays over substrates. The insets show SEM images of the Pt ring and dot arrays printed on the ITO substrates.

The Au nanoring and nanodot arrays printed over ITO glasses:

The SEM images in Figures S7a-b show the Au ring and dot nanoarrays printed on ITO substrates by the CNT and CNP stamps. Figure S7c show representative XRD data for the Au nanorings and nanodots printed on the ITO glasses, indicating that the metal ring and dot arrays are well transferred to the ITO substrates. These printed Au nanoring and nanodot arrays are directly applied to CO oxidation reactions.

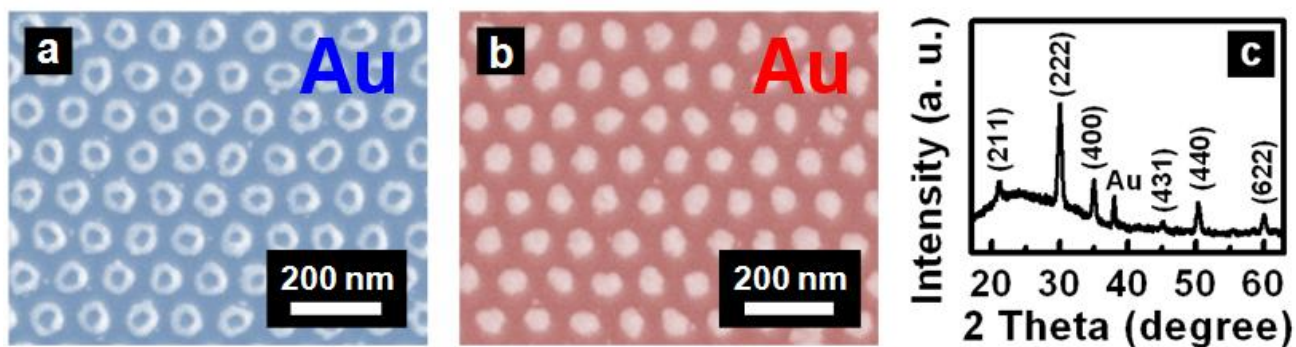


Fig. S7 SEM images of (a) the Au nanorings and (b) the Au nanodots printed over the ITO glasses. (c)

The representative XPD spectra of the Au nanoarrays on the ITO substrates.

The cycling tendency of the printed Au nanoring and nanodot arrays for the CO oxidation:

Figure S8 shows the CV cycling profile of the printed Au nanoring and nanodot arrays in the CO saturated 1.0 M KOH electrolyte solution with continuous CO gas bubbling. In Figure S8, the mass-normalized activity of the Au nanorings remains higher than that of the Au nanodots, but the activity of the ring structures decreases a little faster than that of the dot structures. The CO and CO-like poisoning intermediates are irreversibly adsorbed on the active surface of the catalysts and block the active sites of the catalyst surfaces. Therefore, the catalysts with the higher EAS can easily lose their initial activity for the electrooxidation reactions.^{S1-S3} In our study, the EAS value of the printed nanoring arrays is much larger than the nanodot arrays, leading to the relatively faster decrease of the initial activity.

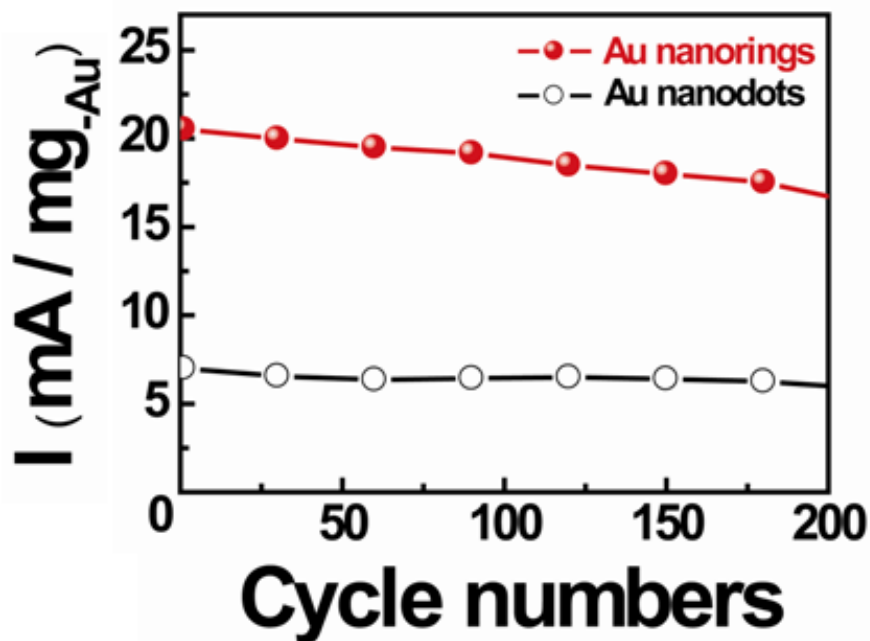


Fig. S8 The cycling tendency of the printed Au nanoring and nanodot arrays in the CO saturated 1.0 M KOH electrolyte solution with continuous CO gas bubbling. All electrocatalytic reactions were carried out between -0.4 to 0.6 V at a scan rate of 100 mV/s.

References

- S1 L. Zhao, Z. -B. Wang, X. -L. Sui, G. -P. Yin, *J. Power Sources* 2014, **245**, 637
- S2 Z. Yao, R. Yue, C. Zhai, F. Jiang, H. Wang, Y. Du, C. Wang, P. Yang, *Int. J. Hydrogen Energy* 2013, **38**, 6368
- S3 X. Li, W. -X. Chen, J. Zhao, W. Xing, Z. -D. Xu, *Carbon* 2005, **43**, 2168